This is a repository copy of *Highly conductive, stretchable, and cell-adhesive hydrogel by nanoclay doping*.

White Rose Research Online URL for this paper:
http://eprints.whiterose.ac.uk/152006/

Version: Published Version

Article:

Tondera, C., Akbar, T.F., Thomas, A.K. et al. (5 more authors) (2019) Highly conductive, stretchable, and cell-adhesive hydrogel by nanoclay doping. Small, 15 (27). ISSN 1613-6810

https://doi.org/10.1002/smll.201901406

Reuse

This article is distributed under the terms of the Creative Commons Attribution-NonCommercial (CC BY-NC) licence. This licence allows you to remix, tweak, and build upon this work non-commercially, and any new works must also acknowledge the authors and be non-commercial. You don't have to license any derivative works on the same terms. More information and the full terms of the licence here: https://creativecommons.org/licenses/

Takedown

If you consider content in White Rose Research Online to be in breach of UK law, please notify us by emailing eprints@whiterose.ac.uk including the URL of the record and the reason for the withdrawal request.

White Rose
university consortium
Universities of Leeds, Sheffield & York

eprints@whiterose.ac.uk
https://eprints.whiterose.ac.uk/

Highly Conductive, Stretchable, and Cell-Adhesive Hydrogel by Nanoclay Doping

*Christoph Tondera, Teuku Fawzul Akbar, Alvin Kuriakose Thomas, Weilin Lin, Carsten Werner, Volker Busskamp, Yixin Zhang, and Ivan R. Minev**

Electrically conductive materials that mimic physical and biological properties of tissues are urgently required for seamless brain–machine interfaces. Here, a multinetwork hydrogel combining electrical conductivity of 26 S m^{-1}, stretchability of 800%, and tissue-like elastic modulus of 15 kPa with mimicry of the extracellular matrix is reported. Engineering this unique set of properties is enabled by a novel in-scaffold polymerization approach. Colloidal hydrogels of the nanoclay Laponite are employed as supports for the assembly of secondary polymer networks. Laponite dramatically increases the conductivity of in-scaffold polymerized poly(ethylene-3,4-diethoxy thiophene) in the absence of other dopants, while preserving excellent stretchability. The scaffold is coated with a layer containing adhesive peptide and polysaccharide dextran sulfate supporting the attachment, proliferation, and neuronal differentiation of human induced pluripotent stem cells directly on the surface of conductive hydrogels. Due to its compatibility with simple extrusion printing, this material promises to enable tissue-mimetic neurostimulating electrodes.

The fusion of biology and electronics requires electrodes implanted inside the body. As part of therapeutic neuroprosthetic systems, they can facilitate restoration of neurological functions lost in injury or disease.[1–3] Their long-term integration inside the brain, spinal cord, or peripheral nerves is still a major challenge. Electrode–tissue interaction often elicits glial scar formation, blood–brain barrier disruption, and electrode degradation.[4,5] This motivates a desire to move beyond traditional materials such as metals and silicon toward conductors that mimic the mechanical and biochemical properties of host tissues. Recent efforts have achieved remarkable biointegration by modeling the viscoelastic properties of electrodes on those of connective tissues surrounding the central nervous system.[6,7] Conductors with elastic moduli of several MPa have been realized using structured thin metal films or polymer–metal composites.[8,9] A truly biomimetic electrode material, however, needs to be even softer and approximate elastic moduli of neural tissues. The ideal material should be soft yet robust to withstand deformation during body movements, handling, and implantation.[10] The electrode needs to form a continuum with the extracellular matrix. Ideally, neurons should make direct connections or be incorporated within its bulk.[11] The conductive material should be compatible with at least one microfabrication technique to enable miniaturization and processing into electrode arrays. As these properties are difficult to achieve with inorganic materials, recent attention has turned to synthetic hydrogels. These share many similarities with tissues, such as high water content, mechanical softness, and specific cell interactions.[12,13] Hydrogels are, however, intrinsically nonelectroconductive. Some promising strategies for their electrical functionalization rely on incorporating conductive polymers such as poly(3,4-ethylenedioxythiophene) doped with polystyrene sulfonate (PEDOT:PSS), polyaniline, or polypyrrole.[14–16] Recently, gelation of aqueous emulsions of PEDOT:PSS nanoparticles using ionic liquids has been reported to produce highly conductive hydrogels that have been integrated in cuff-type sciatic nerve implants in mice.[17,18] When combined with a secondary polymer network for mechanical strength, elastic hydrogels with conductivities above 10 S m^{-1} have been achieved.[19] In another approach, conductive polymers are synthesized from monomers within

---

Dr. C. Tondera, T. F. Akbar, Dr. I. R. Minev
Biotechnology Center (BIOTEC)
Center for Molecular and Cellular Bioengineering (CMCB)
Technische Universität Dresden
Dresden 01307, Germany
E-mail: ivan.minev@tu-dresden.de

T. F. Akbar, Prof. C. Werner
Leibniz Institute of Polymer Research Dresden (IPF)
Max Bergmann Center of Biomaterials Dresden (MBC)
Dresden 01069, Germany

Dr. A. K. Thomas, Dr. W. Lin, Prof. Y. Zhang
B CUBE Center for Molecular Bioengineering
Center for Molecular and Cellular Bioengineering (CMCB)
Technische Universität Dresden
Dresden 01307, Germany

Prof. C. Werner, Dr. V. Busskamp
Center for Regenerative Therapies Dresden (CRTD)
Center for Molecular and Cellular Bioengineering (CMCB)
Technische Universität Dresden
Dresden 01307, Germany

The ORCID identification number(s) for the author(s) of this article can be found under https://doi.org/10.1002/smll.201901406.

© 2019 The Authors. Published by WILEY-VCH Verlag GmbH & Co. KGaA, Weinheim. This is an open access article under the terms of the Creative Commons Attribution-NonCommercial License, which permits use, distribution and reproduction in any medium, provided the original work is properly cited and is not used for commercial purposes.

The copyright line for this article was changed on 18 September 2019 after original online publication.

DOI: 10.1002/smll.201901406

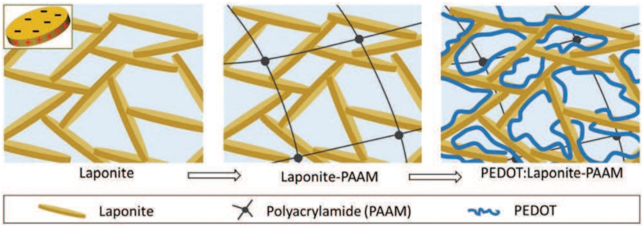

Figure 1. Designer multinetwork hydrogel. The noncovalent Laponite network forms a scaffold for polymerization of functional materials. Polyacrylamide imparts elasticity to the material. PEDOT when doped with Laponite increases conductivity of the final composite.

the scaffold of a pre-existing hydrogel.[14] Achieving high conductivities with this approach requires multiple polymerization steps,[20] additional acid treatment,[21,22] design of self-doping monomers,[23] or the incorporation of secondary dopants.[24] Recent progress in enabling electrical conductivity in hydrogels has outpaced the development of strategies for engineering specific interactions with biological cells.[14,15,18,19,25]

Here, we present a novel approach for the synthesis of tissue-inspired conductive hydrogels. Our approach relies on the separate and sequential polymerization of an elastic and a conductive polymer within a colloidal hydrogel scaffold (**Figure 1**). In the final material, the interpenetrating covalent networks interact with the scaffold contributing to electrical doping and stretchability of the material. A typical hydrogel produced in this way has elastic modulus of 15 kPa, exhibits conductivity of ≈26 S m^{-1}, and survives up to 800% strain electrically and mechanically. Finally, we functionalize the material with a custom, chemically defined biomatrix containing an adhesive peptide and a polysaccharide. We demonstrate the attachment of induced pluripotent stem cell (iPSC) cultures on the surface of the conductive hydrogel and their continuous adhesion during induced neuronal differentiation.

Our hypothesis is that a rationally chosen polymerization scaffold can significantly improve electrical and mechanical properties of a multinetwork hydrogel. As polymerization scaffold we use colloidal dispersions of the smectite nanoclay Laponite. Laponite consists of silicate nanoplatelets ($Na^{0.7+}[(Si_8Mg_{5.5}Li_{0.3})O_{20}(OH)_4]^{0.7-}$) ≈25 nm in width and 0.92 nm in thickness.[26] When dispersed in water, the faces of the platelets become negatively charged while the edges assume a positive charge. Stabilized by electrostatic interactions, nanocrystals form a "house of cards" structure, which conveniently provides spaces for intercalation of functional polymer networks[27,28] (Figure 1). Laponite hydrogels retain their shape unsupported even when consisting of more than 90% water, which together with pronounced shear thinning behavior has found them applications in bioprinting.[27,29,30] They, however, lack the mechanical strength or conductivity needed for use in potential bioelectronic devices. In combination with a second covalently cross-linked polymer, Laponite hydrogels can form composites with toughness that exceeds both that of the neat Laponite and that of the covalent network.[27] To demonstrate this effect, we dissolve acrylamide monomers, *N*,*N*′-methylenebis(acrylamide) (MBAA) cross-linker, and a photoinitiator in the aqueous phase of the Laponite hydrogel. Because the mixture is transparent, we use UV light to cross-link the polyacrylamide (PAAM) network in situ forming Laponite–PAAM hydrogels. Cross-linked polyacrylamide hydrogels have been reported as biocompatible, nontoxic, and nondegradable and have been utilized in clinical applications in vivo as injectable soft tissue fillers.[31–33] As expected, the hybrid Laponite–PAAM hydrogel network exhibits high ultimate tensile strain, in excess of 3000%, significantly higher than that of neat polyacrylamide (Figure S1A, Supporting Information). The elastic modulus of the Laponite–PAAM composite can be tuned by the degree of cross-linking in the covalent network and in our system can be varied in the range of 3.0–22 kPa (Figure S1B, Supporting Information). In experiments that follow, we use Laponite–PAAM hydrogels cross-linked with 0.02% MBAA, exhibiting elastic modulus of 11.4 kPa (10 wt% Laponite, 25 wt% acrylamide, and 0.02 wt% MBAA). First, we investigate whether Laponite–PAAM can serve as a scaffold for preparing conductive polymer PEDOT. Typically, PEDOT requires doping with an anionic polyelectrolyte such as PSS, which improves conductivity and ensures PEDOT:PSS microgels can be dispersed in water.[34] We hypothesize that the Laponite network can act as polymerization scaffold for PEDOT and that negative charges on individual Laponite crystals can dope PEDOT polymer chains similarly to PSS. A direct polymerization of PEDOT in the Laponite–PAAM scaffold, however, is hindered by the low solubility of EDOT monomers in water. To overcome this, we employ an interfacial polymerization method (Figure S2A, Supporting Information). We dissolve the oxidizing agent ammonium persulfate (APS) in the bulk of Laponite–PAAM hydrogels and immerse them in mineral oil containing EDOT monomers. Oxidative polymerization is initiated on the surface of the hydrogels where phase separation ensures APS does not leak into the EDOT bath. Successful polymerization in the hydrogels is indicated by a color change from transparent, to pale blue, to black (**Figure 2**A). Over the course of several hours, slow diffusion of oxidized EDOT monomers into the hydrogel results in PEDOT polymerization in the bulk (Figure S2B, Supporting Information). PEDOT polymerization occurs in both Laponite–PAAM and neat PAAM hydrogels. Fourier-transform infrared (FTIR) spectra of composite hydrogels shown in Figure 2B confirm the successful polymerization of the constituent networks. Bands at ≈1600 cm^{-1} (primary amine) and ≈1640 cm^{-1} (C=O stretching) are attributed to the PAAM network,[35] while bands at ≈1500 cm^{-1} (C=C asymmetric stretching), and ≈1200 and ≈1050 cm^{-1} (C—O—C bending vibrations) are typical of PEDOT.[36] The PEDOT:Laponite–PAAM hydrogel exhibits an additional peak at ≈900 cm^{-1} that is attributed to vibration of the Si—O—Si bonds in Laponite crystals[35] (Figure S3, Supporting Information), which in our case confirms that the colloidal polymerization scaffold remains incorporated in the multinetwork hydrogels.

Next, we investigate the effects of Laponite on the electrical properties of our hydrogels, using impedance spectroscopy, measurements of conductivity (four-probe technique), and cyclic voltammetry. Impedance spectra are obtained by placing hydrogel strips on two gold plate electrodes as illustrated in Figure 2C.[37] We observe that the impedance modulus of PEDOT:Laponite–PAAM hydrogels is at least an order of magnitude lower than that of PEDOT–PAAM hydrogels (and control hydrogels without any PEDOT; Figure S4, Supporting Information) throughout the entire frequency window of 10^0–10^5 Hz. For the Laponite-doped hydrogel, the impedance modulus

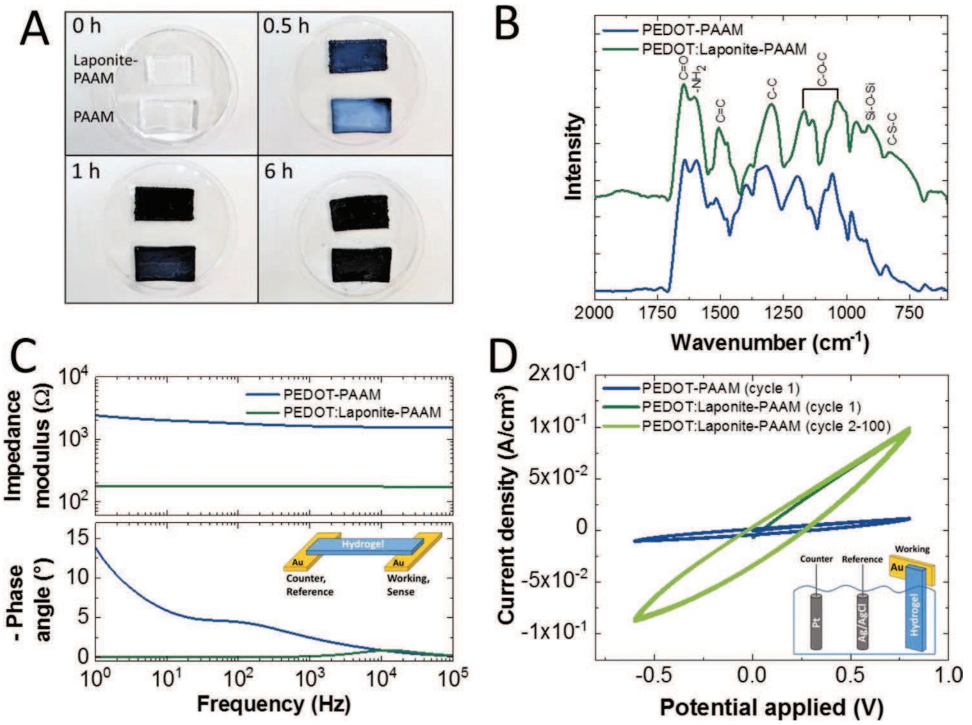

Figure 2. Electrical functionalization. A) After 6 h of polymerization in the EDOT bath, hydrogels turn completely black. B) FTIR spectra of (dried) gels where PEDOT was polymerized in the presence or absence of Laponite. A peak at about 900 cm^{-1} is attributed to the Si—O—Si vibration in Laponite crystals. C) Impedance spectra of PBS swollen hydrogels. The inset illustrates the experimental setup. Hydrogel samples are ≈1 mm thick, 10 mm wide, and the gold plate separation is 35 mm. D) Cyclic voltammetry of PEDOT:Laponite–PAAM and PEDOT–PAAM hydrogels immersed in PBS. Here, current flows out of the hydrogel toward a large platinum counter electrode. Potential scan rate is 50 mV s^{-1}.

shows minimal dependency on frequency and the phase angle remains close to 0°. This behavior is typical of resistors and prompted a direct measurement of conductivity using a four-probe measuring setup. For PEDOT:Laponite–PAAM hydrogels, we measure a conductivity of 26 ± 0.5 S m^{-1} ($n = 3$) that remains stable during a 10 min long test (Figure S5, Supporting Information). We could not obtain conductivity values for the nondoped PEDOT–PAAM samples and hydrogels without PEDOT (Laponite–PAAM and neat PAAM) using this method and instead observed hydrolysis and corrosion on the measuring probes. This indicates that with the exception of the doped PEDOT:Laponite–PAAM, the remaining gels do not support DC conductivity. Our results show that polymerization of PEDOT alone appears to be insufficient to produce highly conductive hydrogels, likely due to the low density of mobile charge carriers typical of neat conductive polymers.[38] We conjecture that the drastically improved conductivity of Laponite-containing hydrogels is due to the introduction of mobile charge carriers (holes) in the PEDOT backbone compensated by negative charges on the surface of Laponite crystals. Conductive PEDOT:Laponite–PAAM hydrogels contain ≈4 times more PEDOT than PEDOT–PAAM hydrogels (Figure S6, Supporting Information). This alone is unlikely to account for the large differences in conductivity, suggesting that Laponite indeed serves to dope the PEDOT backbone. A previous report on PEDOT:PSS/nanoclay composites has not identified any significant effects on conductivity.[39] To our knowledge, this is the first report of the use of a nanoclay for doping of conductive polymers. The conductivity (four-probe) of PEDOT:Laponite–PAAM hydrogels is among some of the highest reported for PEDOT-containing hydrogels.[14,19,20] The percolating scaffold of Laponite nanocrystals in our system ensures PEDOT forms a continuous conductive network. This removes the need for ionic liquids or acid treatment as means of inducing percolation in PEDOT:PSS microgels. We conjecture that similar effects on the conductivity of in-gel polymerized PEDOT can be achieved in other mineral colloid scaffolds, for example, in gels formed by fumed silica particles.[40]

Using PEDOT:Laponite–PAAM and PEDOT–PAAM hydrogels we conduct cyclic voltammetry experiments, where the hydrogel is immersed in phosphate-buffered saline (PBS) and current is forced to flow out of the hydrogel through the electrolyte (Figure 2D).[41] This scenario simulates use of the material in stimulation electrodes that require reversible charge injection.[42] As compared to PEDOT–PAAM, the Laponite-doped material exhibits superior charge injection characteristics. For PEDOT:Laponite–PAAM, anodic and cathodic currents are nearly symmetrical (Figure 2D) and remain unchanged over at least 100 cycles indicating good electrochemical stability. The shape of the voltammogram could be interpreted as a superposition of Ohmic conduction in the hydrogel bulk and capacitive charging/discharging of electrical double layers formed along the interface between PEDOT-rich domains and the electrolyte.[34]

Having established the beneficial effect of Laponite on conductivity, we focus on the PEDOT:Laponite–PAAM hydrogels and study their electromechanical performance. We apply uniaxial strain to record stress–strain curves while

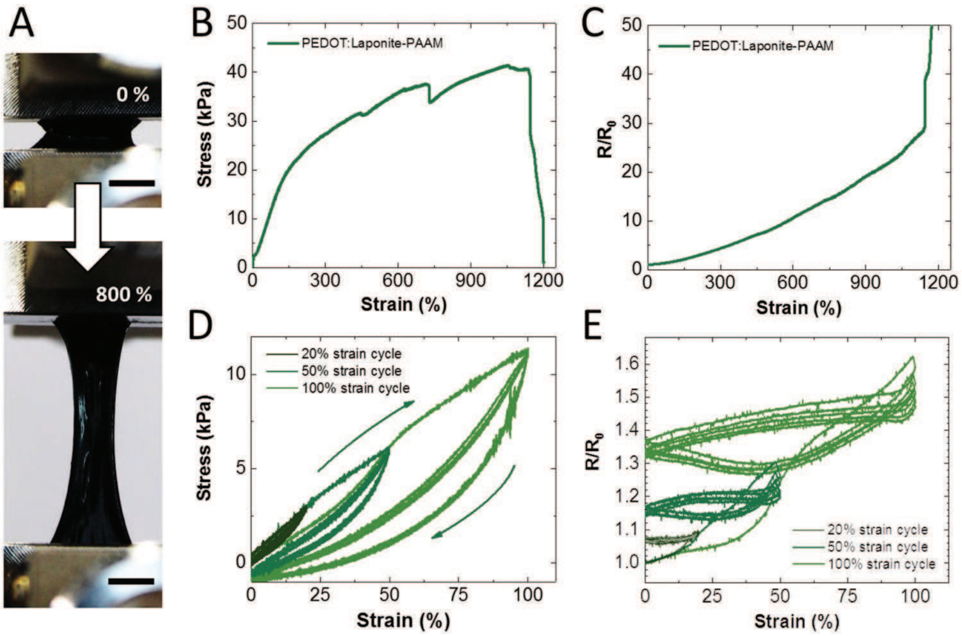

Figure 3. Electromechanical properties of PEDOT:Laponite–PAAM hydrogels. A) Picture of a sample elongated to 800% tensile strain (scale bar = 5 mm). B) Stress–strain (to failure) curve for a representative hydrogel. C) Resistance–strain (to failure) curve for the same sample as in (B). Here, R denotes the instantaneous resistance during strain and R_0 is the initial sample resistance measured after mounting. D) Cyclic stretching to increasing peak strain. E) The corresponding change in resistance measured concurrently. For stretch experiments, sample gauge length is around 4 mm. The strain rate is set at 0.1 mm s^{-1}.

simultaneously measuring electrical resistance. Typical PEDOT:Laponite–PAAM hydrogels survive at least 800% tensile strain before breaking (**Figure 3**A; Figure S7A, Supporting Information). Elastic moduli were calculated in the linear region of the strain–stress response and yield a value of 15 ± 4 kPa (n = 3) (Figure S7B, Supporting Information). This is somewhat higher than values reported for brain tissue (0.1–10 kPa) as summarized in a recent review.[28] However, the range of elasticities of our hydrogels matches well that of substrates used for differentiation of neural precursor cells.[29] Interestingly, PEDOT:Laponite–PAAM hydrogels retain finite electrical conductivity until they break. As illustrated in Figure 3C, even strains as large as 500% produce only a tenfold increase in resistance. High stretchability is unusual for PEDOT:PSS. When processed in thin-film form, it behaves as a brittle solid.[43] Our explanation for the remarkable stretchability of conductive in-gel polymerized PEDOT relates to uncoiling of continuous PEDOT chains within the hydrated Laponite–PAAM matrix. We expected that PEDOT:Laponite–PAAM hydrogels will exhibit stretchability beyond 3000% similar to the tough Laponite–PAAM hydrogels (Figure S1, Supporting Information); however, this is not the case. We conjecture that the interaction of PEDOT chains with Laponite crystals may interfere with electrostatic interactions within the Laponite scaffold. This in turn may modify mechanisms of crack propagation in the composite gel limiting the failure strain.[44]

Energy dissipation mechanisms in hybrid hydrogels can lead to plastic deformation following application of strain.[45] Although PEDOT:Laponite–PAAM hydrogels exhibit pronounced hysteresis (Figure 3D), they recover their original length upon strain relaxation. In subsequent stretch cycles (to the same strain), the material appears weakened, but hysteresis is significantly reduced. This holds for peak strains of at least 100%, which far exceeds strains encountered by biological tissues in vivo. Partial preservation of elastic behavior is attributed to the presence of the covalently cross-linked PAAM network that provides a restoring force. The electrical conductivity of PEDOT:Laponite–PAAM hydrogels is sensitive to the maximum stretch encountered. However, beyond a first (priming) strain cycle, conductivity shows minimal hysteresis and dependence on strain (Figure 3E). Highly conductive hydrogels may find applications as interconnects or as charge injection coatings in ultrasoft multielectrode arrays. Strain invariant conductivity is a desired property, for example, because movement in freely behaving organisms should not induce artifacts in recorded signals.

Integration of conductive hydrogels in devices may be facilitated by additive fabrication technologies such as extrusion 3D printing.[46] As PEDOT:Laponite–PAAM cannot be printed directly, we investigate whether extrusion can be incorporated as an additional step during its preparation. Our strategy is to first pattern Laponite–PAAM structures and use them as scaffolds for subsequent PEDOT polymerization. Laponite–PAAM structures are easily printed because colloidal suspensions containing Laponite exhibit pronounced shear thinning (**Figure 4**A). When finally PEDOT is polymerized in printed scaffolds, some additional swelling is observed (Figure 4B). Thus, the final diameter of PEDOT:Laponite–PAAM fibers is determined by a combination of the material swelling ratio (Figure S8, Supporting Information), the choice of printing nozzle, and its translational speed during printing. The

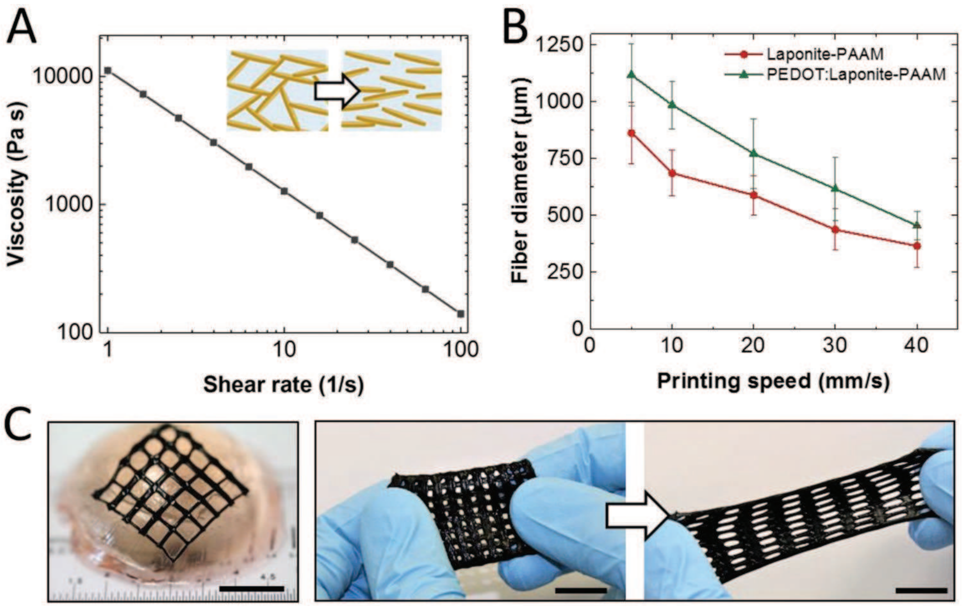

Figure 4. Laponite enables printing of conductive hydrogels. A) Laponite–PAAM pregels exhibit shear thinning under increasing shear rates (mean ± standard deviation, $n = 3$). Inset: shear stress disrupts electrostatic interactions between individual nanocrystals causing the gel to transition to a liquid state. When shear is removed, the material returns to the gel state. B) The diameter of Laponite–PAAM scaffold fibers can be tuned by varying the printing speed. Following polymerization of PEDOT, additional swelling is observed. Printed structures are polymerized and then swollen in PBS for at least 12 h. The printing nozzle has inner diameter of 200 µm. (mean ± standard deviation, $n = 12$). C) Examples of different printed hydrogel meshes are shown. Left panel: PEDOT:Laponite–PAAM adapting to the curvature of a soft gelatin hemisphere. Right panel: printed PEDOT:Laponite–PAAM mesh stretched (scale bar = 10 mm).

thinnest freestanding PEDOT:Laponite–PAAM filaments we could produce with a 200 µm nozzle have diameters of 450 µm after swelling in PBS. A selection of printed structures is presented in Figure 4C. While the patterning resolution offered by direct ink writing will not allow the fabrication of electrode arrays with cell-scale resolution, we point out that many bioelectronic implants in clinical use today require electrode sizes and densities within the reach of mesoscale fabrication technologies such as extrusion 3D printing.[47,48]

Finally, we show that functionalization of PEDOT:Laponite–PAAM hydrogels with a chemically defined biomatrix can transform them from an inert into a highly cell-adhesive biomaterial. As a model cell, we use a human iPSC line where conditional expression of the neurogenic factors Neurogenin-1 and Neurogenin-2 leads to rapid and homogeneous generation of neurons.[49] These neurons mature and become functional in long-term cultures.[50] To select the components of the biomatrix coating, we screen several combinations of adhesive peptides and polysaccharides (screenMATRIX, denovoMATRIX GmbH, Germany; Figure S9, Supporting Information). A combination of the polysaccharide dextran sulfate and a peptide sequence (NGEPRGDTYRAY) from bone sialoprotein (BSP) is observed to support good adhesion and proliferation for the specific iPSC line and is chosen to form the ECM mimicking biomatrix.[51] The biomatrix consists of four-arm polyethylene glycol (starPEG) where each arm is covalently coupled to a peptide containing the BSP adhesive fragment and a lysine-rich sequence $(KA)_7$. The role of the positively charged $(KA)_7$ residue within the BSP–$(KA)_7$–starPEG construct is to bind the negatively charged dextran sulfate. Biomatrices formed via such noncovalent interactions have demonstrated excellent chemical and temporal stability.[52,53] Initially we attempted to immobilize the biomatrix on PEDOT:Laponite–PAAM gels by physical adsorption; however, this did not render gels cell adhesive. To overcome this, we link the BSP adhesive peptide covalently to the hydrogel via silane chemistry. The assembly of the biomatrix on the hydrogel surface proceeds in several steps (Figure S10, Supporting Information). After drying the hydrogels completely, exposed surfaces are activated with air plasma. A silane, (3-aminopropyl)triethoxysilane, is coupled to hydroxyl groups generated on the surface of hydrogels. Using a *N*-(9-fluorenylmethoxycarbonyloxy)succinimide (fmoc) deprotection assay, we establish the quantity of amino groups available for peptide binding on PEDOT:Laponite–PAAM hydrogels as 7.7 nmol mg^{-1} (Figure S11, Supporting Information). Amino groups are then converted to carboxyl groups with succinic anhydride. The BSP–$(KA)_7$–starPEG conjugate is coupled to carboxyl groups on the conductive hydrogel by EDC/sulfoNHS chemistry and finally dextran sulfate is immobilized through noncovalent interaction with lysine residues.[13,54] Biomatrix functionalization did not lead to a significant change in electrical properties. After functionalization, we observe a small resistance decrease of 11%. The putative structure of the biomatrix film is presented in **Figure 5**A. We observe that iPSCs attach and proliferate on the surface of PEDOT:Laponite–PAAM hydrogels functionalized with the biomatrix (Figure 5B) but not on the pristine gel without biomatrix (Figure S12, Supporting Information). Adherent iPSCs expand to form a confluent monolayer in 4 days and maintain their stemness as indicated by expression of the Oct3/4 markers (Figure 5B).

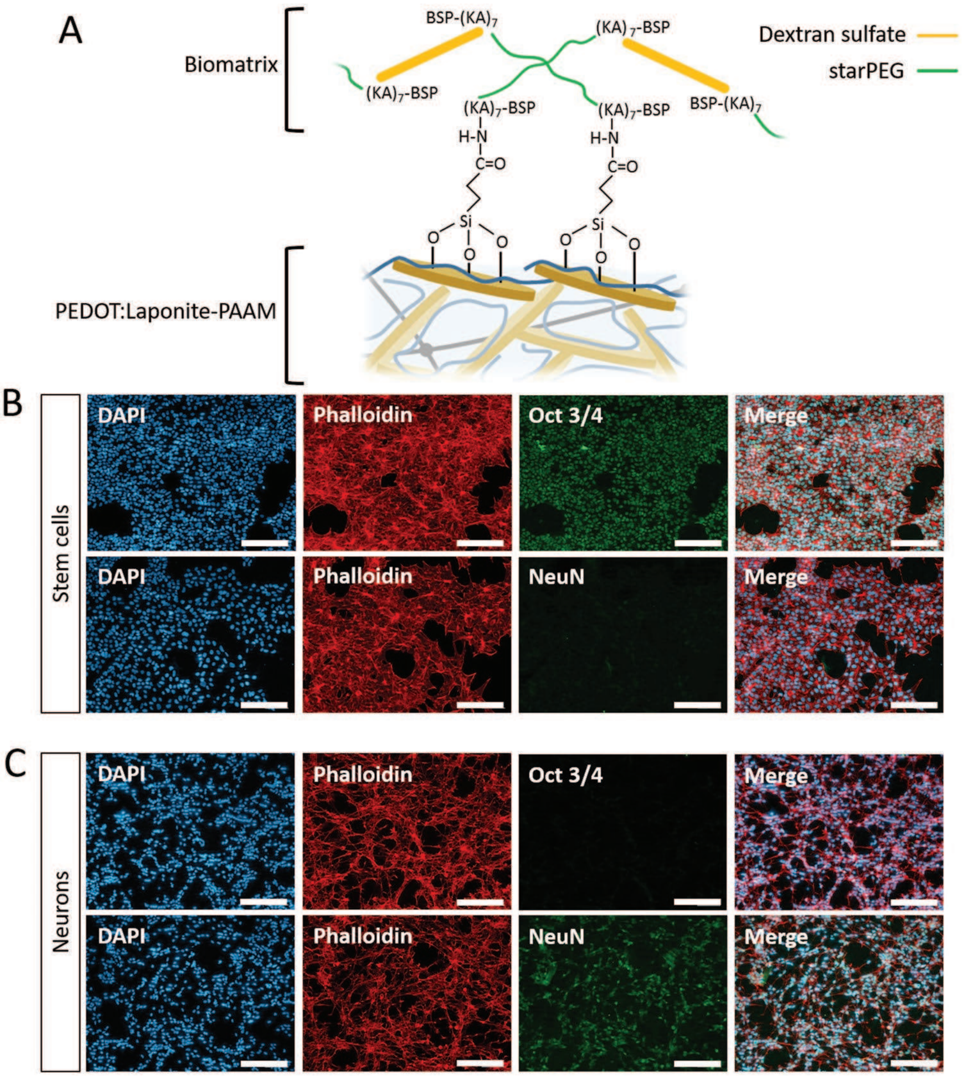

Figure 5. Biomatrix functionalization. A) Scheme illustrating the functionalization of conductive PEDOT:Laponite–PAAM hydrogels. The BSP–(KA)$_7$–starPEG construct is covalently attached via silane coupling. Dextran sulfate is immobilized via electrostatic interaction with (KA)$_7$ residues. B) On functionalized PEDOT:Laponite–PAAM hydrogels, iPSCs attach and retain their stemness as indicated by positive Oct3/4 staining, but show no expression of the neural marker NeuN. C) Conditional expression of the neurogenic factors Neurogenin-1 and Neurogenin-2 leads to expression of the mature neuronal marker NeuN, accompanied by the emergence of axon-like filaments and cessation of Oct3/4 expression. Differentiated cells remain attached to the biomatrix functionalized hydrogel. Color key: blue—cell nuclei; red—actin; and green—antibody stain for Oct 3/4 or NeuN. Scale bar = 200 µm.

Cell monolayers continue to adhere to functionalized PEDOT:Laponite–PAAM surfaces even when differentiated into neuron-like cells expressing the mature neuronal marker NeuN (Figure 5C). We point out that differentiation here is triggered by transcriptional activation of neurogenic factors and not specifically by the conductive properties of the hydrogel. Our aim is to demonstrate that upon suitable choice of functional blocks for the biomatrix, our hydrogel can be engineered to support specific cell adhesion interactions. Since any peptide sequence can be incorporated into the (KA)$_7$–starPEG construct, the conductive surface can be potentially functionalized to modulate its interaction with host tissue. This is expected to be an important factor controlling the foreign body response to chronically implanted electrodes. Further studies are necessary to evaluate the interaction of our material with immune cells and its long-term stability in vivo. Engineering porosity in the bulk may also open applications in 3D cell culture.

In conclusion, we demonstrate the synthesis of multinetwork hydrogels supporting high electrical conductivity, stretchability, and printability. This unique combination of properties is facilitated by the synergistic interaction of nanoclay colloidal dispersions with secondary polymer networks of PEDOT and polyacrylamide. We also demonstrated that a biomatrix composed of rationally selected adhesion components can be integrated with the conductive hydrogel. This functionalization enabled attachment of human iPSCs. Our "cyborganic" approach highlights a promising route toward bringing the gap between electronic and tissue engineering materials for implanted brain–machine interfaces.

Experimental Section

Details of the materials and experimental methods used are available in the Supporting Information.

Supporting Information

Supporting Information is available from the Wiley Online Library or from the author.

Acknowledgements

C.T. and T.F.A. contributed equally to this work. This work was supported through a Freigeist fellowship (91 690, Electronic Tissue Technology for Spinal Cord Repair) from the Volkswagen Foundation and by an ERC starting grant(804005-IntegraBrain) to I.R.M., Leibniz Institute of Polymer Research Dresden (IPF), and Biotechnology Center (BIOTEC) of TU Dresden. V.B. was supported by a Volkswagen Foundation Freigeist fellowship (A110720) from the Volkswagen Foundation and by an ERC starting grant (678071-ProNeurons). The authors would like to thank Petra Welzel for the useful discussions, Mikhail Malanin for FTIR measurements, Evelyn Sauter and Anka Kempe for cell culture protocols and staining, Ulrike Hofmann for fmoc binding assay, and Richard Wetzel for hydrogel functionalization. The authors acknowledge technical support from the Light Microscopy Facility, a Core Facility of the CMCB Technology Platform at TU Dresden and the Analytics Department at IPF Dresden. C.T., T.F.A., A.K.T., and W.L. performed the experiments and data analysis. C.T., T.F.A., A.K.T., C.W., V.B., Y.Z., and I.R.M. designed the study and wrote the manuscript.

Conflict of Interest

The authors declare no conflict of interest.

Keywords

3D printing, bioelectronics, conductive polymers, induced pluripotent stem cells, interpenetrating network

Received: March 15, 2019
Revised: April 11, 2019
Published online: April 26, 2019

---

[1] N. Wenger, E. M. Moraud, J. Gandar, P. Musienko, M. Capogrosso, L. Baud, C. G. Le Goff, Q. Barraud, N. Pavlova, N. Dominici, I. R. Minev, L. Asboth, A. Hirsch, S. Duis, J. Kreider, A. Mortera, O. Haverbeck, S. Kraus, F. Schmitz, J. DiGiovanna, R. van den Brand, J. Bloch, P. Detemple, S. P. Lacour, E. Bezard, S. Micera, G. Courtine, *Nat. Med.* **2016**, *22*, 138.

[2] C. E. Bouton, A. Shaikhouni, N. V. Annetta, M. A. Bockbrader, D. A. Friedenberg, D. M. Nielson, G. Sharma, P. B. Sederberg, B. C. Glenn, W. J. Mysiw, A. G. Morgan, M. Deogaonkar, A. R. Rezai, *Nature* **2016**, *533*, 247.

[3] S. Raspopovic, M. Capogrosso, F. M. Petrini, M. Bonizzato, J. Rigosa, G. Di Pino, J. Carpaneto, M. Controzzi, T. Boretius, E. Fernandez, G. Granata, C. M. Oddo, L. Citi, A. L. Ciancio, C. Cipriani, M. C. Carrozza, W. Jensen, E. Guglielmelli, T. Stieglitz, P. M. Rossini, S. Micera, *Sci. Transl. Med.* **2014**, *6*, 222ra19.

[4] V. S. Polikov, P. A. Tresco, W. M. Reichert, *J. Neurosci. Methods* **2005**, *148*, 1.

[5] J. K. Nguyen, D. J. Park, J. L. Skousen, A. E. Hess-Dunning, D. J. Tyler, S. J. Rowan, C. Weder, J. R. Capadona, *J. Neural Eng.* **2014**, *11*, 056014.

[6] I. R. Minev, P. Musienko, A. Hirsch, Q. Barraud, N. Wenger, E. M. Moraud, J. Gandar, M. Capogrosso, T. Milekovic, L. Asboth, R. F. Torres, N. Vachicouras, Q. Liu, N. Pavlova, S. Duis, A. Larmagnac, J. Vörös, S. Micera, Z. Suo, G. Courtine, S. P. Lacour, *Science* **2015**, *347*, 159.

[7] S. I. Park, D. S. Brenner, G. Shin, C. D. Morgan, B. A. Copits, H. U. Chung, M. Y. Pullen, K. N. Noh, S. Davidson, S. J. Oh, J. Yoon, K.-I. Jang, V. K. Samineni, M. Norman, J. G. Grajales-Reyes, S. K. Vogt, S. S. Sundaram, K. M. Wilson, J. S. Ha, R. Xu, T. Pan, T.-i. Kim, Y. Huang, M. C. Montana, J. P. Golden, M. R. Bruchas, R. W. Gereau, J. A. Rogers, *Nat. Biotechnol.* **2015**, *33*, 1280.

[8] S. Lee, J. Koo, S.-K. Kang, G. Park, Y. J. Lee, Y.-Y. Chen, S. A. Lim, K.-M. Lee, J. A. Rogers, *Mater. Today* **2018**, *21*, 207.

[9] N. Vachicouras, C. M. Tringides, P. B. Campiche, S. P. Lacour, *Extreme Mech. Lett.* **2017**, *15*, 63.

[10] D. E. Harrison, R. Cailliet, D. D. Harrison, S. J. Troyanovich, S. O. Harrison, *J. Manipulative Physiol. Ther.* **1999**, *22*, 322.

[11] J. A. Goding, A. D. Gilmour, U. A. Aregueta-Robles, E. A. Hasan, R. A. Green, *Adv. Funct. Mater.* **2018**, *28*, 1702969.

[12] P. Atallah, L. Schirmer, M. Tsurkan, Y. D. Putra Limasale, R. Zimmermann, C. Werner, U. Freudenberg, *Biomaterials* **2018**, *181*, 227.

[13] R. Wieduwild, R. Wetzel, D. Husman, S. Bauer, I. El-Sayed, S. Duin, P. Murawala, A. K. Thomas, M. Wobus, M. Bornhäuser, Y. Zhang, *Adv. Mater.* **2018**, *30*, 1706100.

[14] S. Wang, C. Sun, S. Guan, W. Li, J. Xu, D. Ge, M. Zhuang, T. Liu, X. Ma, *J. Mater. Chem. B* **2017**, *5*, 4774.

[15] V. Guarino, M. A. Alvarez-Perez, A. Borriello, T. Napolitano, L. Ambrosio, *Adv. Healthcare Mater.* **2013**, *2*, 218.

[16] Y. Shi, L. Pan, B. Liu, Y. Wang, Y. Cui, Z. Bao, G. Yu, *J. Mater. Chem. A* **2014**, *2*, 6086.

[17] M. A. Leaf, M. Muthukumar, *Macromolecules* **2016**, *49*, 4286.

[18] Y. Liu, J. Liu, S. Chen, T. Lei, Y. Kim, S. Niu, H. Wang, X. Wang, A. M. Foudeh, J. B. H. Tok, Z. Bao, *Nat. Biomed. Eng.* **2019**, *3*, 58.

[19] V. R. Feig, H. Tran, M. Lee, Z. Bao, *Nat. Commun.* **2018**, *9*, 2740.

[20] S. Naficy, J. M. Razal, G. M. Spinks, G. G. Wallace, P. G. Whitten, *Chem. Mater.* **2012**, *24*, 3425.

[21] B. Yao, H. Wang, Q. Zhou, M. Wu, M. Zhang, C. Li, G. Shi, *Adv. Mater.* **2017**, *29*, 1700974.

[22] Y. Kim, T. Lim, C.-H. Kim, C. S. Yeo, K. Seo, S.-M. Kim, J. Kim, S. Y. Park, S. Ju, M.-H. Yoon, *NPG Asia Mater.* **2018**, *10*, 1086.

[23] D. Mawad, A. Artzy-Schnirman, J. Tonkin, J. Ramos, S. Inal, M. M. Mahat, N. Darwish, L. Zwi-Dantsis, G. G. Malliaras, J. J. Gooding, A. Lauto, M. M. Stevens, *Chem. Mater.* **2016**, *28*, 6080.

[24] J. Y. Kim, J. H. Jung, D. E. Lee, J. Joo, *Synth. Met.* **2002**, *126*, 311.

[25] Y. Zhou, C. Wan, Y. Yang, H. Yang, S. Wang, Z. Dai, K. Ji, H. Jiang, X. Chen, Y. Long, *Adv. Funct. Mater.* **2019**, *29*, 1806220.

[26] H. Z. Cummins, *J. Non-Cryst. Solids* **2007**, *353*, 3891.

[27] Y. Jin, C. Liu, W. Chai, A. Compaan, Y. Huang, *ACS Appl. Mater. Interfaces* **2017**, *9*, 17456.

[28] L. Han, K. Liu, M. Wang, K. Wang, L. Fang, H. Chen, J. Zhou, X. Lu, *Adv. Funct. Mater.* **2018**, *28*, 1704195.

[29] F. Yang, V. Tadepalli, B. J. Wiley, *ACS Biomater. Sci. Eng.* **2017**, *3*, 863.

[30] S. Hong, D. Sycks, H. F. Chan, S. Lin, G. P. Lopez, F. Guilak, K. W. Leong, X. Zhao, *Adv. Mater.* **2015**, *27*, 4035.

[31] E. Zarini, R. Supino, G. Pratesi, D. Laccabue, M. Tortoreto, E. Scanziani, G. Ghisleni, S. Paltrinieri, G. Tunesi, M. Nava, *Plast. Reconstr. Surg.* **2004**, *114*, 934.

[32] S. von Buelow, N. Pallua, *Plast. Reconstr. Surg.* **2006**, *118*, 85S.

[33] A. D. Kasi, V. Pergialiotis, D. N. Perrea, A. Khunda, S. K. Doumouchtsis, *Int. Urogynecol. J.* **2016**, *27*, 367.
[34] A. V. Volkov, K. Wijeratne, E. Mitraka, U. Ail, D. Zhao, K. Tybrandt, J. W. Andreasen, M. Berggren, X. Crispin, I. V. Zozoulenko, *Adv. Funct. Mater.* **2017**, *27*, 1700329.
[35] S. Skelton, M. Bostwick, K. O'Connor, S. Konst, S. Casey, B. P. Lee, *Soft Matter* **2013**, *9*, 3825.
[36] Q. Zhao, R. Jamal, L. Zhang, M. Wang, T. Abdiryim, *Nanoscale Res. Lett.* **2014**, *9*, 557.
[37] A. R. Spencer, A. Primbetova, A. N. Koppes, R. A. Koppes, H. Fenniri, N. Annabi, *ACS Biomater. Sci. Eng.* **2018**, *4*, 1558.
[38] T. Johansson, L. A. A. Pettersson, O. Inganäs, *Synth. Met.* **2002**, *129*, 269.
[39] A. J. Diaz, H. Noh, T. Meier, S. D. Solares, *Beilstein J. Nanotechnol.* **2017**, *8*, 2069.
[40] S. Mishra, F. J. Scarano, P. Calvert, *J. Biomed. Mater. Res., Part A* **2015**, *103*, 3237.
[41] I. del Agua, D. Mantione, N. Casado, A. Sanchez-Sanchez, G. G. Malliaras, D. Mecerreyes, *ACS Macro Lett.* **2017**, *6*, 473.
[42] S. F. Cogan, *Annu. Rev. Biomed. Eng.* **2008**, *10*, 275.
[43] U. Lang, N. Naujoks, J. Dual, *Synth. Met.* **2009**, *159*, 473.
[44] J.-Y. Sun, X. Zhao, W. R. K. Illeperuma, O. Chaudhuri, K. H. Oh, D. J. Mooney, J. J. Vlassak, Z. Suo, *Nature* **2012**, *489*, 133.
[45] Y. Wang, C. Zhu, R. Pfattner, H. Yan, L. Jin, S. Chen, F. Molina-Lopez, F. Lissel, J. Liu, N. I. Rabiah, Z. Chen, J. W. Chung, C. Linder, M. F. Toney, B. Murmann, Z. Bao, *Sci. Adv.* **2017**, *3*.
[46] A. D. Valentine, T. A. Busbee, J. W. Boley, J. R. Raney, A. Chortos, A. Kotikian, J. D. Berrigan, M. F. Durstock, J. A. Lewis, *Adv. Mater.* **2017**, *29*, 1703817.
[47] R. J. Coffey, *Artif. Organs* **2009**, *33*, 208.
[48] R. B. North, F. T. Wetzel, *Spine* **2002**, *27*, 2584.
[49] V. Busskamp, N. E. Lewis, P. Guye, A. H. Ng, S. L. Shipman, S. M. Byrne, N. E. Sanjana, J. Murn, Y. Li, S. Li, M. Stadler, R. Weiss, G. M. Church, *Mol. Syst. Biol.* **2014**, 10.
[50] R. S. Lam, F. M. Töpfer, P. G. Wood, V. Busskamp, E. Bamberg, *PLoS One* **2017**, *12*, e0169506.
[51] Z. Melkoumian, J. L. Weber, D. M. Weber, A. G. Fadeev, Y. Zhou, P. Dolley-Sonneville, J. Yang, L. Qiu, C. A. Priest, C. Shogbon, A. W. Martin, J. Nelson, P. West, J. P. Beltzer, S. Pal, R. Brandenberger, *Nat. Biotechnol.* **2010**, *28*, 606.
[52] M. V. Tsurkan, K. Chwalek, S. Prokoph, A. Zieris, K. R. Levental, U. Freudenberg, C. Werner, *Adv. Mater.* **2013**, *25*, 2606.
[53] R. Wieduwild, W. Lin, A. Boden, K. Kretschmer, Y. Zhang, *Biomacromolecules* **2014**, *15*, 2058.
[54] A. K. Thomas, R. Wieduwild, R. Zimmermann, W. Lin, J. Friedrichs, M. Bickle, K. Fahmy, C. Werner, Y. Zhang, *ACS Appl. Mater. Interfaces* **2018**, *10*.